Electronic Structure of Epitaxial Single-Layer MoS_2

Jill A. Miwa, Søren Ulstrup, Signe G. Sørensen, Maciej Dendzik, Antonija Grubišić Čabo, Marco Bianchi, Jeppe Vang Lauritsen, and Philip Hofmann*

Department of Physics and Astronomy, Interdisciplinary Nanoscience Center (iNANO), Aarhus University, 8000 Aarhus C, Denmark

(Received 2 October 2014; published 29 January 2015)

The electronic structure of epitaxial single-layer MoS_2 on Au(111) is investigated by angle-resolved photoemission spectroscopy. Pristine and potassium-doped layers are studied in order to gain access to the conduction band. The potassium-doped layer is found to have a (1.39 ± 0.05) eV direct band gap at $\bar{K}$ with the valence band top at $\bar{\Gamma}$ having a significantly higher binding energy than at $\bar{K}$. The moiré superstructure of the epitaxial system does not lead to the presence of observable replica bands or minigaps. The degeneracy of the upper valence band at $\bar{K}$ is found to be lifted by the spin-orbit interaction, leading to a splitting of (145 ± 4) meV. This splitting is anisotropic and in excellent agreement with recent calculations. Finally, it is shown that the potassium doping does not only give rise to a rigid shift of the band structure but also to a distortion, leading to the possibility of band structure engineering in single-layers of transition metal dichalcogenides.

DOI: 10.1103/PhysRevLett.114.046802 PACS numbers: 73.22.-f, 73.20.At, 79.60.-i

Soon after the first isolation of graphene [1–3], it became clear that other layered materials could also be thinned down to a single layer using the same methods, and that such layers may have interesting properties [4]. Particular focus has been on MoS_2 [5–10], a material that had been grown in single layers and used in catalysis even before the advent of graphene [11–14]. Single-layer (SL) MoS_2 has indeed been shown to have a number of intriguing properties. To name but a few, SL MoS_2 has a direct band gap in contrast to the bulk [15] and correspondingly different optical properties [5,6]. Having the conduction band minimum at the $\bar{K}$ point of the Brillouin zone (BZ) opens interesting possibilities for new valley and spin-valley physics [7,9,10]. It is also possible to construct transistors based on SL MoS_2 with the advantage of a high on/off ratio compared to (bilayer) graphene-based devices [8].

Instead of obtaining SL MoS_2 by micromechanical exfoliation, high-quality layers can be grown on different substrates, enabling a new avenue for fundamental investigations of this material. While the growth of nanoscale SL MoS_2 clusters is particularly well established [12,16], it has recently become possible to grow large area epitaxial SL MoS_2 [17]. Similar to many epitaxial graphene systems [18,19], the structure of SL MoS_2 shows a strong moiré superlattice due to the lattice mismatch with the underlying Au(111) [17]. In this Letter, we exploit the very high quality and large areas obtainable for epitaxial SL MoS_2 to study its electronic structure by angle-resolved photoemission spectroscopy (ARPES). This provides a detailed picture of the new effects arising from quantum confinement, breaking of the bulk inversion symmetry, the role of spin-orbit coupling, as well as the effect of the underlying Au(111) and the moiré structure.

Epitaxial SL MoS_2 has been grown on Au(111) by methods described elsewhere [17]. Actually, the total MoS_2 coverage used here was kept somewhat below one monolayer at ≈0.65 ML in order to avoid the growth of bilayer islands that were found to be detectable in ARPES. The epitaxial SL MoS_2 samples are stable in air and could thus be removed from the dedicated growth chamber, transported to the SGM-3 end station on the synchrotron radiation source ASTRID2 [20] and cleaned via mild annealing to 500 K. This procedure has been verified by scanning tunnelling microscopy (STM) to yield atomically clean surfaces. ARPES data were collected at 80 K with an energy and angular resolution better than 20 meV and 0.2°, respectively. All measurements presented here were performed with a photon energy of 49 eV. Even though the band structure of SL MoS_2 is easily distinguished from the photoemission features from the underlying Au(111), photon energy scans were performed to confirm the lack of k_z dispersion of the SL MoS_2 bands.

Figure 1 gives an overview of the epitaxial SL MoS_2 band structure. The constant binding energy cuts in Figs. 1(a)–(d) reveal both Au(111) and SL MoS_2 features. The Au(111)-related states are best identified near the Fermi energy due to the lack of SL MoS_2 states there. We observe the signature of the familiar noble metal Fermi surface as well as a weak and broad signal stemming from the electronic surface state of Au(111) [21]. A more detailed dispersion of this state is shown in the Supplemental Material [22]. At higher binding energies, maxima in the upper valence band (VB) states of SL MoS_2 are observed, both at the $\bar{\Gamma}$ as well as at the $\bar{K}$ points. These features are also seen in the measured dispersion shown in Fig. 1(e). While the states near $\bar{K}$ are very distinct and sharp, those

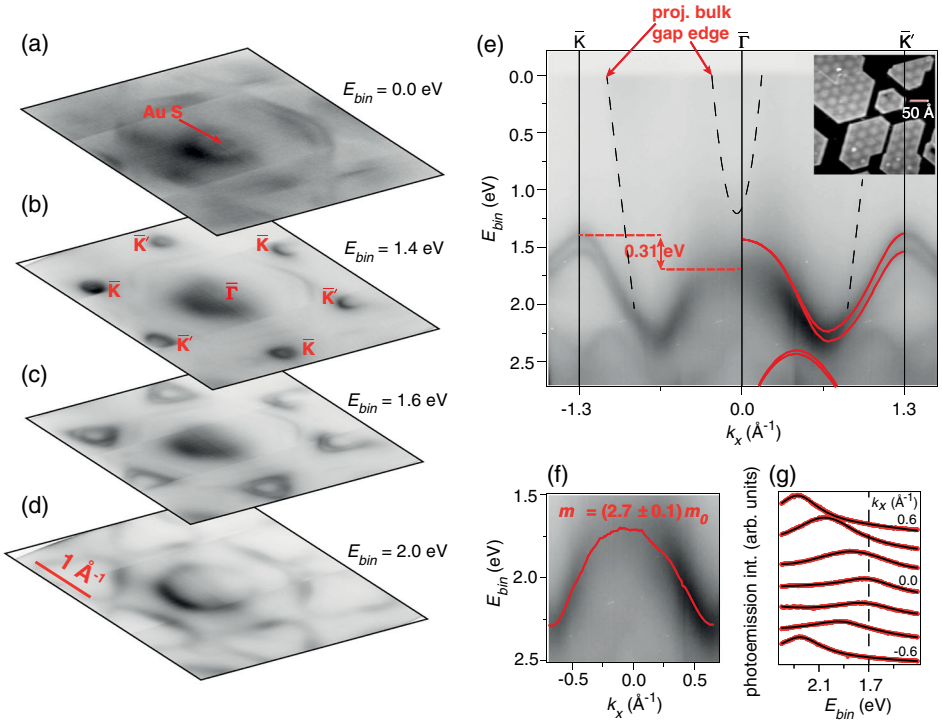

FIG. 1 (color online). Electronic structure of epitaxial single-layer MoS_2: (a)–(d) Constant energy slices through the first Brillouin zone, showing (a) the Fermi contour dominated by Au bulk states and the surface state (Au S) and (b)–(d) evolution of MoS_2 valence band features around $\bar{K}$, $\bar{K}'$, and $\bar{\Gamma}$ points. (e) Valence band dispersion in the $\bar{K}-\bar{\Gamma}-\bar{K}'$ direction. The band structure for freestanding single-layer MoS_2 from Ref. [24] has been superimposed. The inset shows a STM image of the MoS_2 islands and the moiré ($I_t = 0.4$ nA, $V_t = -1.2$ V). (f) Close-up of the MoS_2 upper valence band dispersion around $\bar{\Gamma}$. The red line is the peak position extracted from energy distribution curves shown in (g). The curvature of the parabolic band provides the stated effective mass m in units of the free electron mass m_0. The two-dimensional high-symmetry points in this figure refer to the SL MoS_2 structure.

near $\bar{\Gamma}$ are rather broad [see Figs. 1(f),(g)]. This is ascribed to the different interaction with the substrate and the orbital character of the states. The upper VB near $\bar{K}$ falls into a projected band gap of the Au(111) electronic structure [23] and can therefore not interact with the bulk states. Indeed, the presence of this gap is even visible in the data of Fig. 1(e) as a reduction of background intensity between the Fermi energy and a binding energy of ≈2.2 eV around $\bar{K}$. It is marked by a dashed line. Moreover, the upper VB near $\bar{K}$ is derived from in-plane d- and p-orbitals [24,25] and thus a weak adsorbate-substrate interaction is expected. The upper VB states near $\bar{\Gamma}$, on the other hand, fall within the continuum of projected bulk states [23] and are derived from out-of-plane orbitals [24,25]. For these states a relatively stronger adsorbate-substrate interaction can be expected and this can explain the broadening of the band.

Such an increased interaction is also supported by a comparison of the measured dispersion and the density functional theory band structure for freestanding SL MoS_2 by Zhu *et al.* [24]. In Fig. 1(e), this calculation is superimposed on the data and aligned at the valence band maximum (VBM) at $\bar{K}$. In the calculation, the upper VB maxima at $\bar{K}$ and $\bar{\Gamma}$ are found at nearly the same binding energy. This is also the case for calculations that include many-body effects [26] and in ARPES results from exfoliated SL MoS_2 [27]. Our data, in contrast, show a distortion of the upper VB with the measured maximum at $\bar{\Gamma}$ being 0.31 eV lower than at $\bar{K}$. It is worth noting that the dispersion for exfoliated SL MoS_2 on SiO_2 also deviates from calculation but in a different way: While the VB maxima at $\bar{K}$ and $\bar{\Gamma}$ are aligned, the total width of this band is significantly smaller than in the calculation. Here, on the other hand, the bandwidth agrees very well with the calculation [see Fig. 1(e)].

The observed distortion of the upper valence band near $\bar{\Gamma}$ has only a small effect on the effective mass. A fit to a hole-like parabola [see Figs. 1(f),(g)] gives an effective hole mass of (2.7 ± 0.1) times the free electron mass m_0, in agreement with the calculation for SL MoS_2 ($2.8\ m_0$) [28] and the result for exfoliated SL MoS_2 [$(2.4 \pm 0.3)\ m_0$] [27], but much higher than the bulk value ($0.62\ m_0$) [28].

Another expected consequence of the SL MoS_2-substrate interaction would be a manifestation of the pronounced moiré in the electronic structure. A STM image of the moiré is shown in the inset of Fig. 1(e). A similar moiré has pronounced consequences for the electronic structure of epitaxial graphene, leading to the presence of replica bands and minigaps in the Dirac cone [29,30]. Here, such replicas would be expected at a distance of ≈0.17 Å^{-1} from the main features. We should

easily be able to resolve such features, especially for the sharp bands near $\bar{K}$, but we find them absent from the data, suggesting that the electronic structure of SL MoS_2 is hardly affected by the moiré. We ascribe the difference to graphene to the different character of the states near $\bar{K}$: In graphene, the buckling of the layer directly affects the local interaction of the out-of-plane π orbitals with the substrate. In MoS_2, on the other hand, the bands have a mix of Mo $d_{x^2-y^2}$, d_{xy}, and S p_x, p_y character and are thus totally in-plane. Their local interaction with the substrate can be expected to be less affected by the buckling. Note that this argument does not hold for the upper VB near $\bar{\Gamma}$ where the states have out-of-plane character. While replicas of this band due to the moiré are not observed, we cannot exclude that they contribute to the large width of this band.

A remarkable effect is the strong spin-orbit splitting of the upper VB near $\bar{K}$, shown in greater detail in Fig. 2. Note that the splitting in SL MoS_2 is a genuine lifting of the spin-degeneracy and different from the splitting in the inversion-symmetric bulk material, where it is a combination of layer interaction and spin-orbit coupling and does not remove the spin degeneracy [26]. An equivalent splitting has been observed in ARPES from SL $MoSe_2$ grown on epitaxial graphene [31] but it has so far remained unresolved for exfoliated SL MoS_2 [27]. The size of the splitting can be determined from a fit of the energy distribution curves (EDCs) obtained from the data in Figs. 2(a),(b) and shown in Figs. 2(d),(e). The strongest splitting at $\bar{K}$ is found to be (145 ± 4) meV. This is somewhat bigger than the value of $\approx$100 meV obtained by triply resonant Raman scattering [32] and, as expected, smaller than the ARPES result for SL $MoSe_2$ of 180 meV. It is in excellent agreement with the theoretical prediction of 148 meV from density functional theory [24] and 146 meV from GW calculations [26]. The anisotropy of the splitting away from $\bar{K}$ that gives rise to a triangular warping of the constant energy contours in Fig. 2(c) also agrees with the theoretical prediction [24].

SL MoS_2 is expected to be a semiconductor with a direct band gap at $\bar{K}$, in contrast to the bulk that has an indirect band gap [5,6,15]. Access to the conduction band minimum (CBM) of the SL MoS_2 in ARPES is possible by doping with potassium. This is illustrated in Fig. 3, which shows a series of scans along the $\bar{M}-\bar{K}-\bar{\Gamma}$ and $\bar{A}-\bar{K}-\bar{A}'$ directions of the BZ for the clean surface and increasing exposures to potassium. Overall, the expected strong

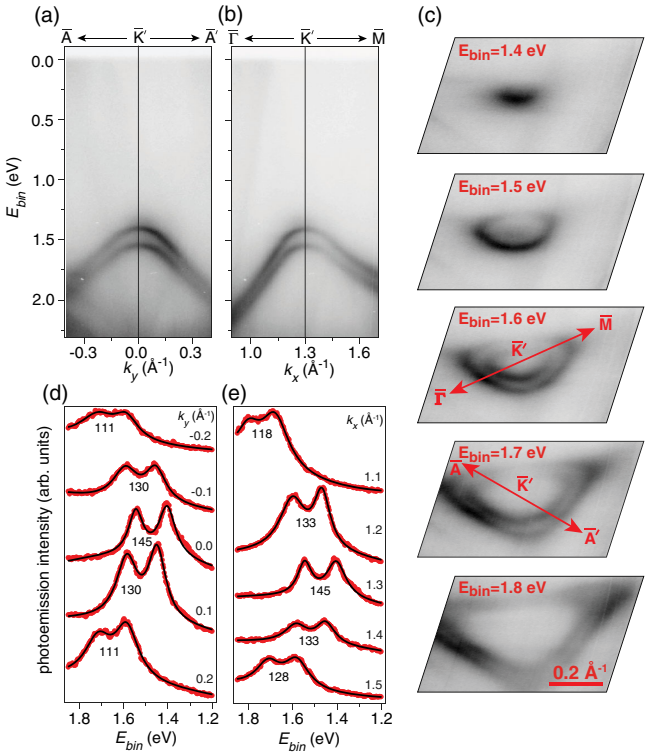

FIG. 2 (color online). Detailed dispersion around valence band maximum at $\bar{K}'$ ($\bar{K}$) and analysis of spin-orbit interaction. (a)–(b) Cuts along directions defined in the constant energy contours in (c). The points $\bar{A}$ and $\bar{A}'$ are along the line perpendicular to the $\bar{\Gamma}-\bar{K}$ direction passing through $\bar{K}$. (d)–(e) EDCs at the given momentum values. The peaks are fitted by a double Lorentzian function, and the difference between peak positions is taken as the splitting of the bands, which is stated in meV below the curves.

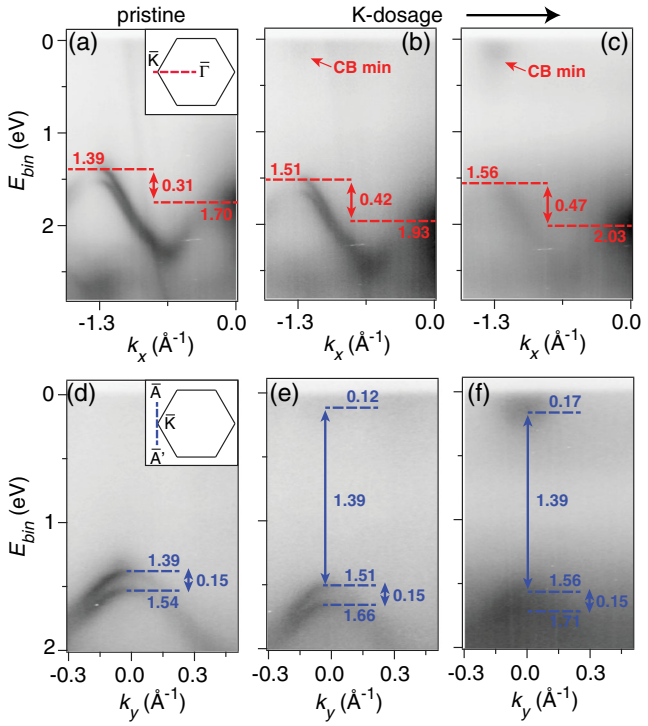

FIG. 3 (color online). Tuning of the band structure by potassium adsorption. (a),(d) Clean sample, (b),(e) first dose, and (c), (f) second dose. The scan directions for the cuts in (a)–(c) and (d)–(f) are given in the insets of (a) and (d), respectively. The points $\bar{A}$ and $\bar{A}'$ are defined in the caption of Fig. 2. The energies are given in eV.

electron doping is indeed observed: For a small potassium dose, all bands are shifted to higher binding energies and a weak photoemission intensity due to the conduction band minimum at $\bar{K}$ becomes observable [Figs. 3(b) and (e)]. As the doping is increased, the CBM becomes populated, demonstrating the direct band gap of the material, as the VBM is also at $\bar{K}$ [Figs. 3(c) and (f)]. The CBM is found to be rather broad, in contrast to the VBM at $\bar{K}$, consistent with the out-of-plane character of these states [24,25]. We determine the gap energy to be (1.39 ± 0.05) eV, substantially smaller than the value of 1.88 eV determined by photoluminescence [5].

We assign the observed band-gap reduction to the vicinity of the metallic support of the layer and the thereby enhanced screening. This effect has been studied theoretically by placing SL MoS_2 onto (insulating) BN and (conductive) graphene and this change leads to a band-gap reduction of $\approx$0.5 eV, in good agreement with our observations here [33]. Experimentally, the effect has been probed for SL $MoSe_2$ that was grown on both bilayer graphene and bulk graphite [34]. In this case, the effect is not as drastic because both substrates are conductive, but it still leads to a band-gap reduction of $\approx$0.24 eV for the more conductive bulk graphite.

Upon closer inspection of Fig. 3, it becomes clear that potassium adsorption does not give rise to a simple rigid shift of the band structure to higher binding energies: While the VBM at $\bar{K}$ shifts by 1.39 eV $-$ 1.56 eV $= -0.17$ eV from the clean sample to the highly potassium-dosed situation, the maximum at $\bar{\Gamma}$ shifts by 1.70 eV $-$ 2.03 eV $= -0.33$ eV, such that the upper VB is severely distorted upon doping. These shifts, together with the observed distortion of the upper VB in the undoped case and the reduced band gap, can all be accounted for by the orbital character of the states involved: Both the upper VB at $\bar{\Gamma}$ as well as the CB minimum at $\bar{K}$ are predominantly of out-of-plane $d_{3z^2-r^2}$ character [24,25] and these states are found to shift to higher binding energy upon either interaction with the substrate or exposure to adsorbed alkali atoms. It is this shift that already deforms the upper valence band near $\bar{\Gamma}$ for the pristine SL MoS_2 on Au(111) and this deformation is merely enhanced upon potassium adsorption. A significantly distorted upper valence band was also found for transferred SL MoS_2 on oxidized Si [27]. In that case, the distortion is quite different in that it leads to a narrowing of the entire band with the energies at $\bar{\Gamma}$ and $\bar{K}$ almost at the same energy. This distortion was also ascribed to the MoS_2-substrate interaction.

The strong dependence of the band maximum at $\bar{\Gamma}$ on the substrate can be understood in the following simple picture: The transition from an indirect to a direct band gap in MoS_2 upon the reduction to a SL has been ascribed to a quantum confinement effect [5,6]. An inspection of the band structure for a different number of layers shows that the confinement-induced energy changes are strongest for the upper valence band maximum at $\bar{\Gamma}$ [6]. In fact, the confinement has a much stronger effect on these states than on the conduction band minimum near $\bar{K}$, despite the similar orbital character. The energy of such quantum-confined states does not only depend on the thickness of the film but also on the wave function's phase shift at the boundaries, i.e., at the MoS_2-substrate and MoS_2-vacuum interfaces [35]. This explains the sensitivity of the VBM at $\bar{\Gamma}$ on the character of the substrate and also on the modification of the vacuum interface upon doping.

In conclusion, we have studied the electronic structure of epitaxial single-layer MoS_2 on Au(111). We find this to give rise to sharp bands, in particular for the VBM near the $\bar{K}$ point and these bands are minimally affected by the presence of the substrate or moiré. This is very different from the π band in epitaxial graphene and we ascribe this to the different orbital character of the bands (in-plane for MoS_2 versus out-of-plane for graphene). We directly observe the strong spin splitting of the upper VB and the size of this is in excellent agreement with theoretical predictions. Upon doping the layer with potassium, we are able to determine the band gap and find that the doping-induced shifts in energy are strongly dependent on the orbital character of the bands. This opens interesting possibilities to intentionally tune the band structure of SL MoS_2 and similar materials. The effect also needs to be taken into account when placing SL MoS_2 between other materials or when doping it by an electric field.

We gratefully acknowledge financial support from the VILLUM Foundation, The Danish Council for Independent Research, the Lundbeck Foundation, The Danish Strategic Research Council (CAT-C) and Haldor Topsøe A/S.

*philip@phys.au.dk

[1] K. S. Novoselov, A. K. Geim, S. V. Morozov, D. Jiang, Y. Zhang, S. V. Dubonos, I. V. Grigorieva, and A. A. Firsov, Science **306**, 666 (2004).
[2] K. S. Novoselov, A. K. Geim, S. V. Morozov, D. Jiang, M. I. Katsnelson, I. V. Grigorieva, S. V. Dubonos, and A. A. Firsov, Nature (London) **438**, 197 (2005).
[3] Y. B. Zhang, Y. W. Tan, H. L. Stormer, and P. Kim, Nature (London) **438**, 201 (2005).
[4] K. S. Novoselov, D. Jiang, F. Schedin, T. J. Booth, V. V. Khotkevich, S. V. Morozov, and A. K. Geim, Proc. Natl. Acad. Sci. U.S.A. **102**, 10451 (2005).
[5] K. F. Mak, C. Lee, J. Hone, J. Shan, and T. F. Heinz, Phys. Rev. Lett. **105**, 136805 (2010).
[6] A. Splendiani, L. Sun, Y. Zhang, T. Li, J. Kim, C.-Y. Chim, G. Galli, and F. Wang, Nano Lett. **10**, 1271 (2010).
[7] T. Cao *et al.*, Nat. Commun. **3**, 887 (2012).
[8] B. Radisavljevic, A. Radenovic, J. Brivio, V. Giacometti, and A. Kis, Nat. Nanotechnol. **6**, 147 (2011).
[9] H. Zeng, J. Dai, W. Yao, D. Xiao, and X. Cui, Nat. Nanotechnol. **7**, 490 (2012).

[10] D. Xiao, G.-B. Liu, W. Feng, X. Xu, and W. Yao, Phys. Rev. Lett. **108**, 196802 (2012).
[11] H. Topsøe, B. S. Clausen, and F. E. Massoth, *Hydrotreating Catalysis*, Catalysis—Science and Technology, Vol. 11 (Springer Verlag, Berlin, 1996).
[12] S. Helveg, J. V. Lauritsen, E. Lægsgaard, I. Stensgaard, J. K. Nørskov, B. S. Clausen, H. Topsøe, and F. Besenbacher, Phys. Rev. Lett. **84**, 951 (2000).
[13] J. Lauritsen, M. Nyberg, R. Vang, M. Bollinger, B. Clausen, H. Topsoe, K. Jacobsen, E. Laegsgaard, J. Norskov, and F. Besenbacher, Nanotechnology **14**, 385 (2003).
[14] T. F. Jaramillo, K. P. Jorgensen, J. Bonde, J. H. Nielsen, S. Horch, and I. Chorkendorff, Science **317**, 100 (2007).
[15] M. V. Bollinger, J. V. Lauritsen, K. W. Jacobsen, J. K. Nørskov, S. Helveg, and F. Besenbacher, Phys. Rev. Lett. **87**, 196803 (2001).
[16] J. V. Lauritsen, J. Kibsgaard, S. Helveg, H. Topsoe, B. S. Clausen, E. Laegsgaard, and F. Besenbacher, Nat. Nanotechnol. **2**, 53 (2007).
[17] S. G. Sørensen, H. G. Füchtbauer, A. K. Tuxen, A. S. Walton, and J. V. Lauritsen, ACS Nano **8**, 6788 (2014).
[18] C. Berger *et al.*, J. Phys. Chem. B **108**, 19912 (2004).
[19] A. T. N'Diaye, J. Coraux, T. N. Plasa, C. Busse, and T. Michely, New J. Phys. **10**, 043033 (2008).
[20] S. V. Hoffmann, C. Søndergaard, C. Schultz, Z. Li, and P. Hofmann, Nucl. Instrum. Methods Phys. Res., Sect. A **523**, 441 (2004).
[21] F. Reinert, G. Nicolay, S. Schmidt, D. Ehm, and S. Hüfner, Phys. Rev. B **63**, 115415 (2001).
[22] See Supplemental Material at http://link.aps.org/supplemental/10.1103/PhysRevLett.114.046802 for a detailed dispersion of the Au(111) surface state.
[23] N. Takeuchi, C. T. Chan, and K. M. Ho, Phys. Rev. B **43**, 13899 (1991).
[24] Z. Y. Zhu, Y. C. Cheng, and U. Schwingenschlögl, Phys. Rev. B **84**, 153402 (2011).
[25] E. Cappelluti, R. Roldán, J. A. Silva-Guillén, P. Ordejón, and F. Guinea, Phys. Rev. B **88**, 075409 (2013).
[26] T. Cheiwchanchamnangij and W. R. L. Lambrecht, Phys. Rev. B **85**, 205302 (2012).
[27] W. Jin *et al.*, Phys. Rev. Lett. **111**, 106801 (2013).
[28] Th. Böker, R. Severin, A. Müller, C. Janowitz, R. Manzke, D. Voß, P. Krüger, A. Mazur, and J. Pollmann, Phys. Rev. B **64**, 235305 (2001); H. Peelaers and C. G. Van de Walle, Phys. Rev. B **86**, 241401 (2012).
[29] A. Bostwick, T. Ohta, T. Seyller, K. Horn, and E. Rotenberg, Nat. Phys. **3**, 36 (2007).
[30] I. Pletikosic, M. Kralj, P. Pervan, R. Brako, J. Coraux, A. T. N'Diaye, C. Busse, and T. Michely, Phys. Rev. Lett. **102**, 056808 (2009).
[31] Y. Zhang *et al.*, Nat. Nanotechnol. **9**, 111 (2014).
[32] L. Sun *et al.*, Phys. Rev. Lett. **111**, 126801 (2013).
[33] H.-P. Komsa and A. V. Krasheninnikov, Phys. Rev. B **86**, 241201 (2012).
[34] M. M. Ugeda *et al.*, Nat. Mater. **13**, 1091 (2014).
[35] T. C. Chiang, Surf. Sci. Rep. **39**, 181 (2000).